N95-14561

# BUBBLE DYNAMICS, TWO-PHASE FLOW, AND BOILING HEAT TRANSFER IN A MICROGRAVITY ENVIRONMENT

Jacob N. Chung
Department of Mechanical and Materials Engineering
Washington State University
Pullman, WA 99164-2920

## ABSTRACT

The two-phase bubbly flow and boiling heat transfer in microgravity represents a substantial challenge to scientists and engineers and yet there is an urgent need to seek fundamental understanding in this area for future spacecraft design and space missions. At Washington State University, we have successfully designed, built and tested a 2.1 second drop tower with an innovative airbag deceleration system. Microgravity boiling experiments performed in our 0.6 second Drop Tower produced data and flow visualizations that agree with published results and also provide some new understanding concerning flow boiling and microgravity bubble behavior. On the analytical and numerical work, the edge effects of finite divergent electrode plates on the forces experienced by bubbles were investigated. Boiling in a concentric cylinder under microgravity and an electric field was numerically predicted. We also completed a feasibility study for microgravity boiling in an acoustic field.

## INTRODUCTION

The thermo-fluid dynamics of two-phase system in microgravity encompass a wide range of complex phenomena that are not well enough understood for engineering design to proceed. Yet there is an urgent need to explore these phenomena for future spacecraft design and space mission. Predicting the two-phase flow and boiling heat transfer phenomena under a microgravity environment requires a thorough understanding of a multitude of fundamental physical processes including bubble dynamics, fluid dynamics, heat transfer, and interfacial transport. Significant gains in microgravity boiling science may result from investigating both the complexities of these phenomena in isolation and when acting in consort.

The current research concentrates on the bubble nucleation, bubble dynamics and heat transfer mechanism under microgravity. Specifically, we intend to study the transport mechanisms when the dominance of buoyancy force is replacd by a velocity shear force, an electro-magnetic force or an acoustical force under the microgravity condition.

## EXPERIMENTATION

### A. WSU 0.6 Second and 2.1 Second Drop Towers

The original purpose of the 0.6 second drop tower was to serve as a 1/4 scale model for the design and construction of the "WSU 2.1 Second Drop Tower." However, with proper planning, it was able to accommodate short time microgravity experiments and has been used extensively as a testing facility for new ideas and experimental designs. The drop distance of this drop tower is 2.13 meters tall which provides a drop time of 0.6 second. The dimensions of the airbag are 45.72 cm x 45.72 cm x 91.44 cm. The maximum deceleration level of the experiment is approximately 3g's. The low gravity level was calculated to be approximately $10^{-3}$ g. The WSU 0.6 second Airbag Drop Tower consists of three major parts: a release-retrieve mechanism, a drag shield, and a airbag deceleration system. Figure 1 shows an overall view of the drop tower.

An empty elevator shaft located in Eastlic Hall on the Washington State University campus was converted to a 2.1 second drop tower facility. The use of a drag shield combined with an innovative airbag deceleration system, and a tapered pin release mechanism provides low gravitational acceleration (~ $10^{-4}$g), very low impact deceleration (~ 15g), and low release vibrations (~ ±5g). Its ability to drop an experiment from a variable height sets it apart from any other drop tower in the world today, and can provide a 1.2 second drop with as little as 5-8g deceleration. A typical g-level history curve for a full 2.1 second drop is shown in figure 2. This can be compared to a deceleration level of 70g as reported for the obsolete sand box system at the NASA Lewis Research Center.

The drop tower was designed with a combined release-retrieve mechanism that can drop a 317 kg load (181 kg drag shield, 136 kg experiment) from any height up to 22 meters and remotely retrieve the experiment within 10 minutes. An innovative airbag deceleration system uses a 1.82 x 2.13 x 3.66m airbag to create the required 20,000 to 35,000 Newton force required to decelerate the experiment after its fall and subsequent 74 km/hr impact. The drop tower was designed to accept the standard experimental "rigs" that are presently used at the NASA Lewis Research Center, making their experiments compatible with our tower. A user-friendly, Windows-based drop and data acquisition program (PULSE) was written to control the entire drop tower operation. This software allows complete control over the release mechanism, and up to 11 other pieces of equipment. This program is also capable of collecting data on 7 input channels, provides simple control over all data acquisition requirements, immediately plots a control curve for each channel used, calculates means and standard deviations for each channel, can write the data to a file or can copy the data directly to the clip board for use in a widows based program. This drop tower's low cost of construction and operation, relative ease of fabrication, and ability to be completely controlled by one person from the drop level makes it ideal for the university environment and for the research at hand. Figure 3 shows an overall view of the drop tower (not to scale).

## B. Preliminary Experimental Results

We have performed pool and flow boiling experiments in the 0.6 second drop tower. The results of the transient boiling experiment show that for a short period of time, when the heat flux is relatively low and the subcooling level remains relatively high, the heat transfer is enhanced in microgravity. At a high enough heat flux, however, dryout would happen almost immediately under microgravity condition and cause the heat transfer to decrease. These results are in good agreement with the study by Merte, Lee, and Ervin [1]. We also found that the increase in heat flux would decrease as the total heat flux becomes higher. At the highest heat flux of 8 $W/cm^2$ dryout occurred and it actually decreased the heat transfer. Figure 4 presents a sample of these results with comparisions to the the work of Merte, Lee, and Ervin [1].

In the comparison between experiments of the same heat flux level with and without forced flow, the low heat flux cases (2.88 $W/cm^2$) result in an increased heat flux with the flow (7.7cm/s). With the medium heat flux (4.17 $w/cm^2$), the flow does not affect the heat flux very much. With the high heat flux (5.95 $w/cm^2$), there was some evidence that the flow field prevents dryout, however, the short times involved limited our insight. In the short time available only the higher heat fluxs have enough time to cause dryout, and if more time were available the dryout might have also been observed for the medium heat flux. However, this probably would not be the case for the low heat flux as the bubbles were immediately removed by the flow field as discussed below. The results in the highest heat flux (8 $W/cm^2$) experiment show dryout occurred in less than 0.1 second after the drop and the heat flux decreased dramatically.

The flow visualization study shows that with a low heat flux, the vapor bubbles are carried by the flow and roll across the heater surface. With a higher heat flux the forced flow provided by the system does not seem to overcome the surface tension. The forced flow therefore does not remove the vapor bubbles from the surface for these higher heat flux cases.

The increase in heat flux under microgravity may be attributed to:

1. The surface tension effects at the liquid-vapor-solid interface causing rewetting to occur and maintaining the nucleate boiling [1].
2. More fresh liquid is available at the heater surface as a result of the liquid inertia which continues to bring the fresh liquid toward the heater surface while the induced upward flow of liquid is stopped when the bubbles do not rise off the heater surface.
3. The thinning of the superheated microlayer.
4. The increase in microlayer evaporation rate resulting from the sliding of the vapor bubble caused by the forced flow [2].
5. The sliding of the vapor bubbles causing agitation on the surface, which creates more nucleation sites and therefore enhances the nucleate boiling.

The results of the current study showed good agreement with previous reports and provided a better understanding for future research. Figure 5 provides typical flow visualization photographs.

## NUMERICAL AND ANALYTICAL ANALYSIS

### A. Electric Field

On the numerical and analytical side, we have investigated the edge effects of a finite plate on the dielectrophoretic force experienced by a gas bubble in a dielectric fluid. We also looked into the bubble growth and dynamics in a concentric cylinder under an electric field.

The dielectrophoretic force on a spherical bubble in an electric field is given as

$$\boldsymbol{F}_{DEP} = 2\pi R^3 \varepsilon_l \left( \frac{\varepsilon_v - \varepsilon_l}{\varepsilon_v + 2\varepsilon_l} \right) \nabla |\boldsymbol{E}|^2 \qquad (1)$$

and for the divergent plates

$$\nabla |\boldsymbol{E}|^2 = \frac{-2}{r^3} \left( \frac{\partial V}{\partial \phi} \right)^2 \qquad (2)$$

Where R is the radius of the bubble, $\boldsymbol{E}$ is the strength of the electric field, $\varepsilon_l$ and $\varepsilon_v$ are the dielectric permittivity for the liquid and vapor phase respectively, and $\phi$ and r are the angular and radial coordinate, respectively. For two divergent infinite plate electrodes with voltages V and -V respectively, the following is obtained:

$$\nabla |\boldsymbol{E}|^2 = \left( \frac{-2V^2}{r^3 \theta^2} \right) \quad , \quad \boldsymbol{F}_{DEP} = -4\pi R^3 \varepsilon_l \left( \frac{\varepsilon_v - \varepsilon_l}{\varepsilon_v + 2\varepsilon_l} \right) \left( \frac{V^2}{r^3 \theta^2} \right) \hat{r} \qquad (3),(4)$$

Where r is the distance from the fictitious plate intersection and $\theta$ is the angle between the two plates.

For finite plates, the general expression for the voltage at any point is:

$$V(\boldsymbol{r}) = \iint_S \frac{\rho(\boldsymbol{r}')ds'}{4\pi\varepsilon_o |\boldsymbol{r} - \boldsymbol{r}'|} \qquad (5)$$

Where S is the surface of object over which charge exists, $\rho(\boldsymbol{r})$ is the charge density at position $\boldsymbol{r}$, $\varepsilon$ is the dielectric permittivity of the medium between the plates and $|\boldsymbol{r} - \boldsymbol{r}'|$ is the distance between $\boldsymbol{r}'$ and $\boldsymbol{r}$. The charge density is not known priori to begin with for the finite plates. However, with the voltage on the plates known, the moment method was employed to solve the integral equations for the charge density. The voltage at each point allows the calculation of the electric field and gradients of the electric field. This is the final information which is needed in order to find the dielectrophoretic force.

Figure 6 presents the DEP force over the entire calculated area for both finite and infinite cases and for a test fluid of R-113. In these plots z = 0 corresponds to the center of the plate and z=1.9 corresponds to the edge of the plate. Also the plots are for $\phi = 0$ (center of the plates).

Because of its higher practical application value, microgravity boiling in a concentric cylinder was investigated by numerical simulations. The simulation covers the bubble growth, bubble detachment from the heater surface and bubble dynamics and movement in an electric field after detachment. The bubble growth starts from the isobaric stage where the heat transfer is the governing mechanism. The bubble is assumed to remain in the shape of a segmented sphere with a constant contact angle. The heat for bubble growth is supplied by the heater surface through a conduction thermal boundary layer to reach the bubble. The detachment is based on a criterion proposed by Fritz [3],

$$Bo^{1/2} = 0.0208\phi \qquad (6)$$

Where

$$Bo = \frac{g(\rho_l - \rho_v)d_d^{\,2}}{\sigma} \quad \text{is the Bond Number} \qquad (7)$$

In the above $\phi$ is the contact angle, $\sigma$ is the surface tension coefficient g is the gravitation acceleration, $\rho_l$ and $\rho_v$ are the densities for the liquid and vapor respectively and $d_d$ is the bubble detachment diameter. After detachment, the bubble dynamics and movement are tracked by the following equation of motion for the bubble:

$$(M+M')\frac{d\mathbf{U}}{dt}=\frac{1}{32}C_D\rho_l{}^2\pi R^2U^2\mathbf{e}_U+\frac{3}{8}\sqrt{\pi\rho_l\mu_l}R^2\int_0^1\frac{\mathbf{U}}{\sqrt{t-t'}}dt'+2\pi R^3\varepsilon_1\frac{\varepsilon_2-\varepsilon_1}{\varepsilon_2+2\varepsilon_1}\nabla E+Mg \qquad (8)$$

In the above equation, M is the mass of the bubble, M' is the added mass due to the acceleration of the surrounding fluid, which is approximated as half of M, $C_D$ is the drag coefficient, $\mu_l$ is the fluid viscosity, and R is the bubble radius. The first term on the right-hand-side is the drag force, Basset force is the second term, the dielectrophoretic force is represented by the third term and the gravitational force is shown in the last term. The numerical method employed to obtain the dielectric force is similar to that for the divergent plates and therefore will not be repeated here. Results for water and R-113 are included in Figure 7.

B. Acoustic Field

A lot more work is still needed in order to really understand all of the physics of how acoustic radiation pressure can be applied in moving vapor bubbles. To this date we have numerically derived all the factors that are required in the the design of a working experiment. With a simple static force balance of buoyancy, surface tension, and radiation force we have shown that an acoustic force produced by a high intensity ultrasonic horn can move vapor bubbles off a heater surface. Finally, an acoustic boiling chamber has been designed based on the numerical calculations. This chamber will form one module of the Enhanced Pool and Flowing Boiling Experiment (EPFBE-1) presently being built for the 2.1 second drop tower. Experiments are planned for summer 1994. The components of interest are the rectangular resonant acoustic chamber, the high intensity ultrasonic horn, and a nicrome wire with working fluid FC-72.

ACKNOWLEDGMENTS

Research assistants for project are Trevor Snyder, Tien-Chen Wang, Ying-Yao Hwang, Yi-Chung Su, and Jeff Sitter. Engineering Shop at WSU did an excellent service for the drop tower and experimental apparatus.

REFERENCES

1. H. Merte, Jr., H.S. Lee, and J.S. Ervin, Transient Nucleate Pool Boiling in Microgravity - Some Initial Results, Int. Symp. Microgravity Science and Applications, Paper J-5, 1993.

2. Tsung-Chang, G. and Bankoff, S.G., On the Mechanism of Forced-Convection Subcooled Nucleate Boiling, J. Heat Transfer, Vol. 112, pp. 213-218, 1990.

3. Fritz, W. Maximum Volume of Vapor Bubbles, Physik Zeitschr, Vol. 36, pp. 379-384, 1935.

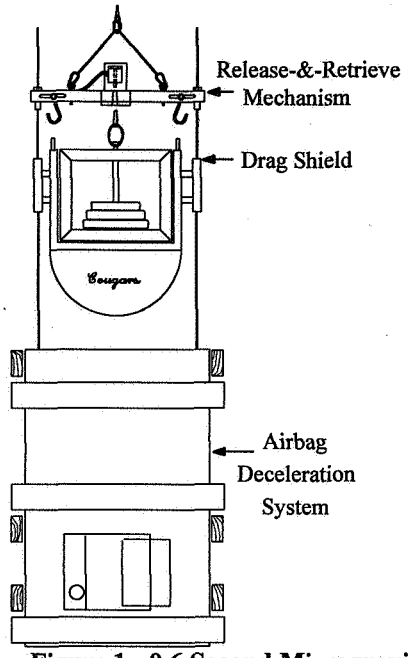


**Figure 1 - 0.6 Second Microgravity Drop Tower**

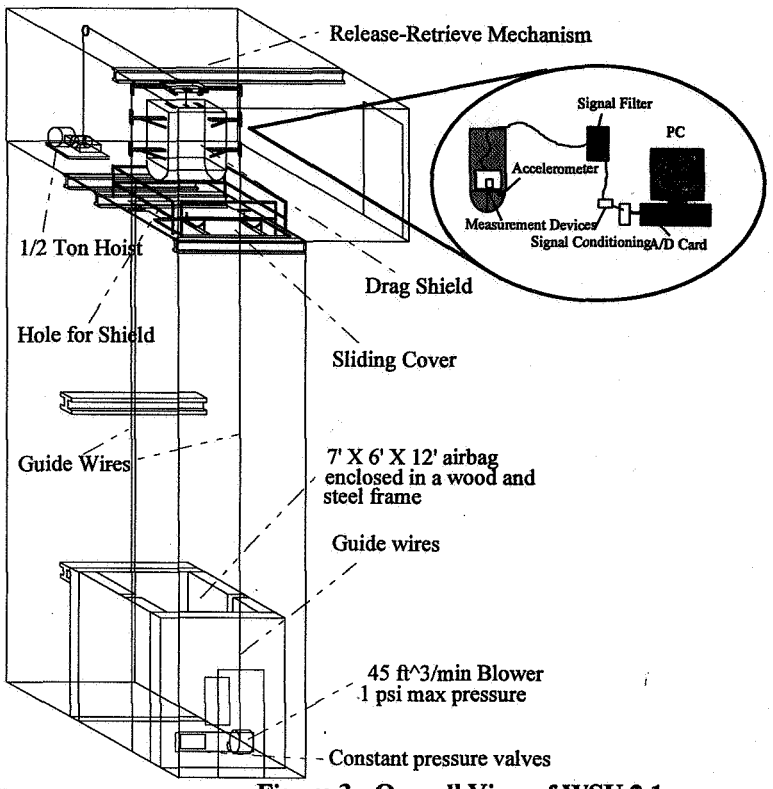


**Figure 3 - Overall View of WSU 2.1 Second Drop Tower**

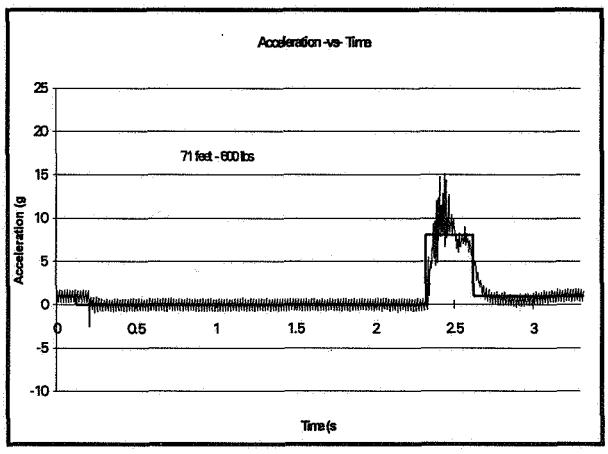


**Firgure 2 - G-level History Curve Acceleration -vs- Time**

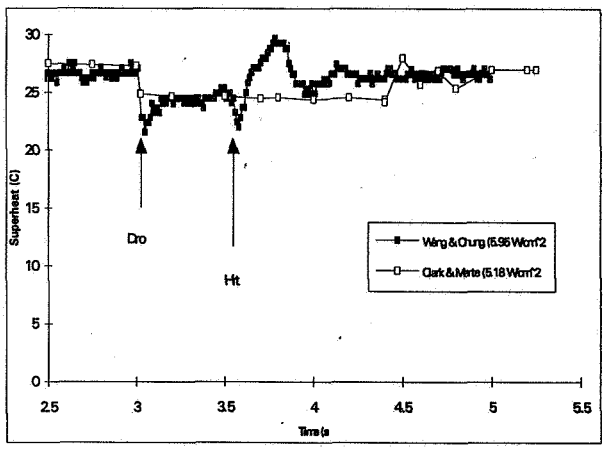


**Figure 4 - Heater Surface Superheat Pool Boiling - R-113**

7.6 W/cm^2 - Microgravity boiling with and without flow

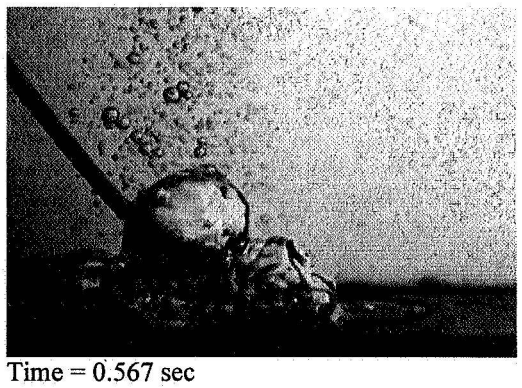

Time = 0.567 sec
Velocity = 0 cm/s

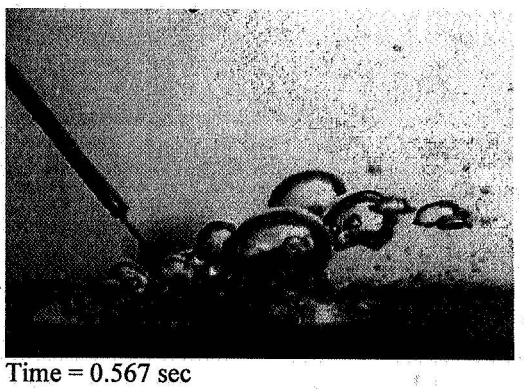

Time = 0.567 sec
Velocity = 7.7 cm/s

2.8 W/cm^2 - Microgravity boiling with and without flow

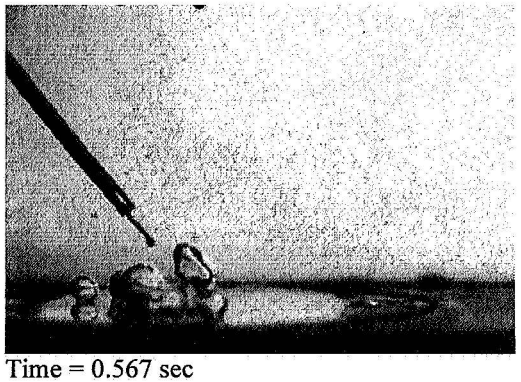

Time = 0.567 sec
Velocity = 0 cm/s

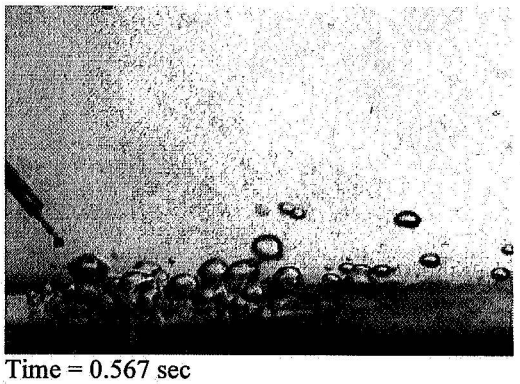

Time = 0.567 sec
Velocity = 7.7 cm/s

**Figure 5 - Microgravity Boiling Flow Visualization photographs**

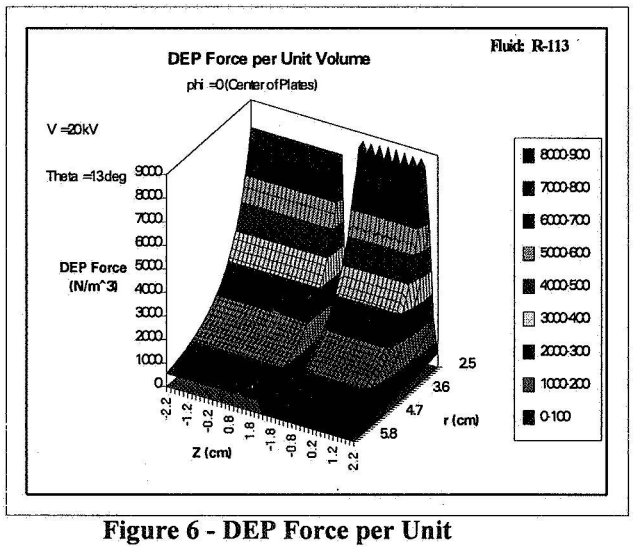


**Figure 6 - DEP Force per Unit Volume Across Finite Plate and Infinite Plate**

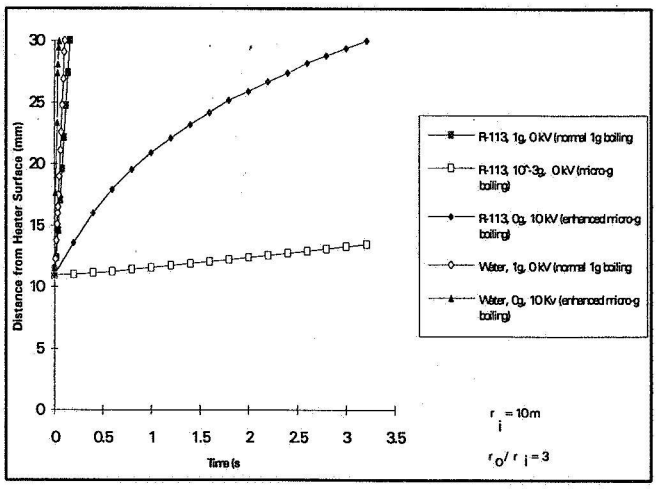


**Figure 7 - Bubble Motion After Detachment**